Full-Duplex Communication on the Shared Channel of a Capacitively Coupled Power Transfer System

Yu-Gang Su, *Member, IEEE*, Wei Zhou, Aiguo Patrick Hu, *Senior Member, IEEE*, Chun-Sen Tang, *Member, IEEE*, Shi-Yun Xie, and Yue Sun, *Member, IEEE*

***Abstract*—This paper proposed a novel wireless power transfer system with full-duplex communication on a shared channel for capacitively coupled power transfer systems. For the analysis of power and signal transmission, a frequency-domain model of the power and signal channels is established. Based on this model, the signal transfer characteristic of the channel and the influence of power flow on the signal channel are analyzed. Moreover, to ensure the power and signal transfer without unacceptable interference or attenuation, a parameters selection method of the communication channel is developed. In addition, an interference suppression strategy by taking the interference from the ipsilateral channel into consideration is proposed. To suppress the interference effectively, an estimation of the ipsilateral channel output signal is made. Then, the signal from the opposite channel is demodulated by removing the estimated values of the interference. Both simulation and experimental results showed have proven the correctness and effectiveness of the proposed wireless power and signal transfer method. Finally, it has demonstrated that the designed channel can transfer 100 W of power, and a full-duplex communication can be well achieved with different data rates in two directions when both two data rates are set within 200 kb/s.**

***Index Terms*—Capacitively coupled power transfer (CCPT), interference suppression, power-signal parallel transmission, wireless power transfer (WPT).**

I. Introduction

RECENTLY, wireless power transfer (WPT) technologies have already attracted broad attention of researchers in the world, and some WPT systems have been applied in many fields [1]–[7]. Capacitively coupled power transfer (CCPT) is a WPT technology which has been applied in rotating devices [8], [9], mobile robots [10], biological implants [11], cell phones [12], as well as electric vehicles [13]–[16]. With capacitive plates in the coupling structure, CCPT has many advantages such as design flexibility, reduced volume and weight of coupling structure, and metal penetration ability [17]. Fig. 1 shows a block diagram of a typical CCPT system.

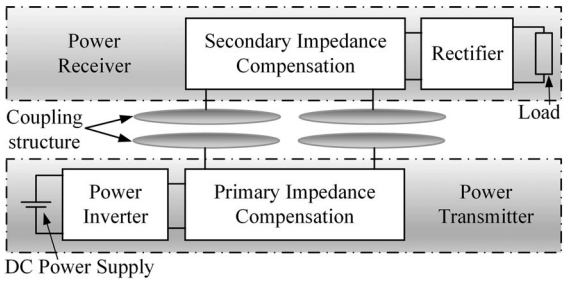

Fig. 1. Block diagram of a typical CCPT system.

One challenge for CCPT system is to achieve large amounts of output power and high power efficiency [18]–[22], and a signal communication system between transmitter and receiver sides can help achieve it, such as tracking the optimal power or efficiency point by transferring load information to the transmitter side and transferring switching frequency to the variable compensation components in the receiver side. Besides, some practical applications inherently require signal communication between transmitter and receiver sides, such as systems with feedback controllers, rotary motors, medical telemeters, special measurement devices [9], [23], [24], etc.

Some wireless signal transmission strategies have been proposed for WPT systems. Wu *et al.* proposed a wireless power and data transfer system via a common inductive link. The power and data transfer share the same inductive link between coreless coils. A reduced signal coupling inductance is adopted in this paper to suppress the power interference caused by the external noise from the power transfer circuit [25]. However, in this power interference suppression method, the SNR can only be increased by magnifying the output of the data carrier. Su *et al.* proposed a power- and signal-shared channel design method which can help achieve the half-duplex communication on CCPT systems. But this method does not suit the channel design for full-duplex communication conditions [26]. Up to now, there is no literature presents methods to realize the full-duplex communication and eliminate the interactions between the two signal sources at each side of the system for simultaneous bi-directional communication on CCPT systems.

This paper presents research results on full-duplex communication on a shared channel of a CCPT system. First, a novel topology for power-signal parallel transmission system is proposed. This topology establishes two weakly coupled links to

Manuscript received November 11, 2015; revised February 20, 2016 and April 27, 2016; accepted May 30, 2016. Date of publication June 14, 2016; date of current version January 20, 2017. This work was supported by the research funds for the National Natural Science Foundation of China under Grant 51477020, Grant 51277192, and Grant 61573074. Recommended for publication by Associate Editor J. M. Rivas Davila.

Y.-G. Su and Y. Sun are with the Key Laboratory of Dependable Service Computing in Cyber Physical Society (Chongqing University), Ministry of Education, Chongqing 400044, China, and also with the College of Automation, , Chongqing University, Chongqing 400044, China (e-mail: su7558@qq.com; syue06@cqu.edu.cn).

W. Zhou, C.-S. Tang, and S.-Y. Xie are with the College of Automation, Chongqing University, Chongqing 400044, China (e-mail: zhouwei_cq@163.com; cstang@cqu.edu.cn; yunshixie@qq.com).

A. P. Hu is with the Department of Electrical and Computer Engineering, University of Auckland, Auckland 1142, New Zealand (e-mail: a.hu@auckland.ac.nz).

Digital Object Identifier 10.1109/TPEL.2016.2580607

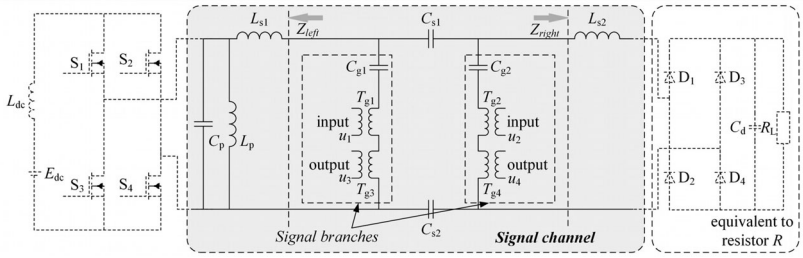

Fig. 2. Proposed topology of the CCPT system with full-duplex communication module.

transfer power and signal, respectively. A full-duplex communication function for CCPT systems is realized while transferring power simultaneously. Second, because of the interference between two signal sources in full-duplex communication system, an ipsilateral signal interference suppression method is proposed to realize a full-duplex communication which is suitable for different carrier frequencies and signal transmission rates of two signal sources at each side.

This paper is organized as follows. In Section II, the topology of power-signal parallel transmission system is proposed. In Section III, according to the topology in Section II, the model of two signal channels in the proposed topology is established and analyzed successively. In Section IV, a parameters selection method of signal channel is presented. In Section V, a steady-state response of interference is estimated to suppress the signal interference from the ipsilateral side. Based on this estimation, a suppression strategy is introduced to demodulate the useful signal from opposite channel. The proposed method is verified by both MATLAB simulations and experimental results. Validation and concluding remarks are presented in Sections VI and VII, respectively.

II. Proposed Topology

Fig. 2 shows the proposed topology of a CCPT system with full-duplex communication on the shared channel. A typical topology for wireless power transmission which includes a full-bridge inverter, a resonant tank, two coupling plates, and a rectifier is adopted. The full-bridge inverter transforms the dc voltage $E_{\rm dc}$ into a high-frequency ac voltage by using four MOSFETs $\rm S_1-S_4$. $L_{\rm dc}$ serves as a dc inductor to form a quasi-current source. The combination of C_p and L_p forms a parallel resonance tank. Under normal operations, two pairs of metal plates on coupling structure can be modeled as a couple of equivalent capacitors C_{s1} and C_{s2}. To transfer power to the load sufficiently, the series coupling capacitors are tuned by the compensation inductors L_{s1} and L_{s2}. The rectifier bridge formed by D_1–D_4 converts the ac voltage into dc for driving the load directly.

To realize the full-duplex communication based on the proposed CCPT topology, a couple of signal branches are connected directly on the metal plates on each side of the system. In each signal branch, one tightly coupled transformer $T_{g1}(\rm T_{g2})$ is employed to load the signal into the signal channel. As such, the signal in the channel is picked up and detected by another tightly coupled transformer ($T_{\rm g3}/\rm T_{g4}$). In addition, the capacitors C_{g1} and C_{g2} serve as isolation capacitors which isolate low-frequency power wave transfer across the signal branch. To keep the power flow out of the signal channel effectively, the values of capacitors C_{g1} and C_{g2} have to be set to be low since the ac signal wave at a high frequency can transfer across capacitors C_{g1} and C_{g2} easily.

As for the signal channel, the combination of quasi-current source and full-bridge inverter serves as an ac current source which is equivalent to an open circuit. Moreover, an equivalent ac resistance *R* can be used to replace the rectifier, filter capacitor C_d, and load R_L [27]. The signal channel is shown in Fig. 2 and the proposed topology in Fig. 2 contains many inductors and capacitors which result in a complicated high-order channel. Therefore, a simplified signal channel should be established to analyze the channel characteristic. For power transfer, the components of the resonance tank satisfy

$$\begin{cases} \omega_p^2 L_p C_p - 1 = 0 \\ \omega_p^2 \left(L_{s1} + L_{s2}\right) \dfrac{C_{s1} C_{s2}}{C_{s1} + C_{s2}} - 1 = 0 \end{cases} \tag{1}$$

where ω_p is the undamped natural angular frequency of the power resonance tank. Generally, the signal frequency is much higher than the frequency of power resonance tank. The signal angular frequency $\omega_{\rm s}$ can be expressed as

$$\omega_s = \lambda \omega_p \ \ (\lambda \gg 1) \tag{2}$$

where λ is the ω_s/ω_p ratio. Define the impedances on the left side of the primary signal branch and the right side of secondary signal branch as $Z_{\rm left}$ and $Z_{\rm right}$, respectively, and the expression of these two impedances can be obtained in (3), and a complete derivation is provided in the Appendix

$$\begin{cases} Z_{\rm right} = j\omega_s L_{s2} \\ Z_{\rm left} = j\omega_s L_{s1} \end{cases}. \tag{3}$$

Then, the signal channel can be simplified to a symmetrical structure as shown in Fig. 3.

In Fig. 3, there are four signal channels named $\rm S_{A-C}, S_{A-D}, S_{B-C}, S_{B-D}$, respectively. The subscript label of each channel name indicates the input and output ports. For example, $\rm S_{A-C}$ represents the channel with the input-port Port A, and output-port Port C. Set L_{s1} equals L_{s2}, C_{g1} equals C_{g2} and four tightly coupled transformers are all the same, then the model of communication in both directions becomes the same. The

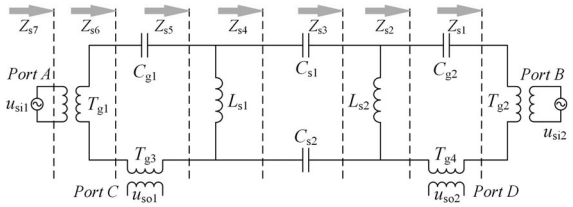

Fig. 3. Simplified circuit of signal channel on the CCPT system.

channel S_{A-C} and S_{B-D} are equivalent and named as ipsilateral channels. Similarly, the channel S_{A-D} and S_{B-C} are equivalent as well, and they are named as opposite channels.

III. Modeling and Analysis

Generally, for the power and signal parallel transmission in the proposed system, three factors, namely the gains of signal channels, gain of power channel, and the power interference on signal channel, should be taken into consideration. Therefore, three corresponding models are established in this paper as follows.

A. Gains of Signal Channels

As for the topology in Fig. 3, to calculate the gains of signal channels more easily, the circuit is divided into seven parts with certain impedances which are shown in (4)

$$\begin{cases} Z_g = j\omega_s L_g + R_g \\ Z_{s1} = \dfrac{(\omega_s M_g)^2}{Z_g} + Z_g \\ Z_{s2} = \dfrac{1}{j\omega_s C_{g2}} + Z_{s1} + Z_g \\ Z_{s3} = \dfrac{j\omega_s L_{s2} Z_{s2}}{j\omega_s L_{s2} + Z_{s2}} \end{cases}, \quad \begin{cases} Z_{s4} = \dfrac{C_{s1} + C_{s2}}{j\omega_s C_{s1} C_{s2}} + Z_{s3} \\ Z_{s5} = \dfrac{j\omega_s L_{s1} Z_{s4}}{j\omega_s L_{s1} + Z_{s4}} \\ Z_{s6} = Z_{s5} + \dfrac{1}{j\omega_s C_{g1}} + Z_g \\ Z_{s7} = \dfrac{(\omega_s M_g)^2}{Z_{s6} + Z_g} + Z_g \end{cases} \tag{4}$$

where Z_{s1}, Z_{s2}, Z_{s3}, Z_{s4}, Z_{s5}, Z_{s6}, and $\mathrm{Z_{s7}}$ represent the impedance of each part which are shown in Fig. 3. Z_g denotes the impedance of single siding coil of the tightly coupled transformer. Besides, L_g, R_g, and M_g are defined as the self-inductance, internal resistance, and mutual inductance of the tightly coupled transformer, respectively. According to the Kirchhoff Voltage and Current Law (KVL and KCL), the transfer function of each part can be expressed as

$$\begin{cases} G_{s1} = \dfrac{i_{\mathrm{si1}}}{u_{\mathrm{si1}}} = \dfrac{1}{Z_{s7}} \\ G_{s2} = \dfrac{i_{Cg1}}{i_{\mathrm{si1}}} = \dfrac{j\omega_s M_g}{Z_{s6} + Z_g} \\ G_{s3} = \dfrac{u_{\mathrm{so1}}}{i_{Cg1}} = j\omega_s M_g \\ G_{s4} = \dfrac{u_{Ls1}}{i_{Cg1}} = Z_{s5} \end{cases}, \quad \begin{cases} G_{s5} = \dfrac{i_{Cs1}}{u_{Ls1}} = \dfrac{1}{Z_{s4}} \\ G_{s6} = \dfrac{u_{\mathrm{Ls2}}}{i_{Cs1}} = Z_{s3} \\ G_{s7} = \dfrac{i_{\mathrm{Cg2}}}{u_{\mathrm{Ls2}}} = \dfrac{1}{Z_{s2}} \\ G_{s8} = \dfrac{u_{\mathrm{so2}}}{i_{\mathrm{Cg2}}} = j\omega_s M_g \end{cases} \tag{5}$$

where i_{si1} and u_{si1} are the current and voltage of the signal source, u_{so1} and u_{so2} are the voltage of the signal output port without power transmission, i_{Cg1}, i_{Cs1}, i_{Cg2} are the current of the C_{g1}, C_{s1}, and C_{g2}, respectively. u_{Ls1}, u_{Ls2} represent the voltages of the L_{s1} and L_{s2}.$G_{\mathrm{si}}(i=1,2,3,\ldots,8)$ represent the transfer functions of intermediate variables of i_{si1}, i_{Cg1}, u_{Ls1}, i_{Cs1}, u_{Ls2} and i_{Cg2} in (5) which are adopted to simplify the solving process and solution. Based on (4) and (5), the transfer functions from signal source voltage u_{si1} to the voltage of two signal output ports u_{so1} and u_{so2} can be obtained as

$$\begin{cases} G_{\mathrm{ipsilateral}} = \dfrac{u_{\mathrm{so1}}}{u_{\mathrm{si1}}} = \displaystyle\prod_{i=\{1,2,3\}} G_{\mathrm{si}} \\ G_{\mathrm{opposite}} = \dfrac{u_{\mathrm{so2}}}{u_{\mathrm{si1}}} = \displaystyle\prod_{i=\{1,2,4,5,6,7,8\}} G_{\mathrm{si}} \end{cases}. \tag{6}$$

The transfer functions $G_{\mathrm{ipsilateral}}$ and G_{opposite} represent the signal gain functions of the ipsilateral and opposite channels, respectively. They are adopted to evaluate the gains of two signal channels.

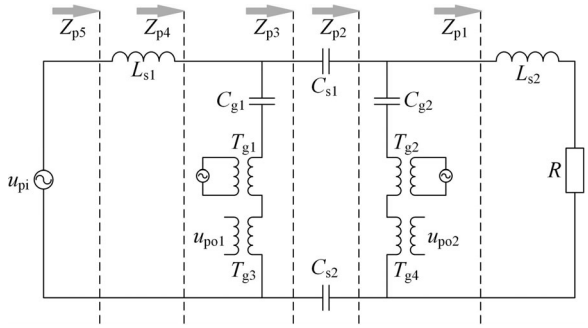

Fig. 4. Simplified circuit of power channel of the CCPT system.

B. Gain of Power Channel and Power Interference on Signal Channel

Fig. 4 shows the power channel of the proposed topology. Consider the voltage u_{pi} on the parallel resonant tank as the input power source of the system, the gain of power channel can be represented by the transfer function from u_{pi} to the voltage across the load resistor *R*. Besides, the power interference on signal channel can be calculated by the transfer function from u_{pi} to the voltage on two signal output ports u_{po1} and u_{po2}. All these transfer functions are excited by only the voltage u_{pi}, without signal input.

To calculate these transfer functions more easily, the circuit is divided into five parts with certain impedances which are shown below

$$\begin{cases} Z_g = j\omega_p L_g + R_g \\ Z_{b1} = \dfrac{(\omega_p M_g)^2}{Z_g} + 2Z_g + \dfrac{1}{j\omega_p C_{g1}} \\ Z_{b2} = \dfrac{(\omega_p M_g)^2}{Z_g} + 2Z_g + \dfrac{1}{j\omega_p C_{g2}} \\ Z_{p1} = j\omega_p L_{s2} + R \end{cases}, \quad \begin{cases} Z_{p2} = \dfrac{Z_{b2} Z_{p1}}{Z_{b2} + Z_{p1}} \\ Z_{p3} = \dfrac{C_{s1} + C_{s2}}{j\omega_p C_{s1} C_{s2}} + Z_{p2} \\ Z_{p4} = \dfrac{Z_{b1} Z_{p3}}{Z_{b1} + Z_{p3}} \\ Z_{p5} = j\omega_p L_{s1} + Z_{p4} \end{cases} \tag{7}$$

where Z_{p1}, Z_{p2}, Z_{p3}, Z_{p4}, and Z_{p5} represent the impedance of each part which are shown in Fig. 4. Z_{b1} and Z_{b2} indicate the impedance of signal branches at transmitter and receiver side, respectively. According to KVL and KCL, the transfer function of each part can be expressed as

$$\begin{cases} G_{p1} = \dfrac{i_{Ls1}}{u_{\mathrm{pi}}} = \dfrac{1}{Z_{p5}} \\ G_{p2} = \dfrac{u_{b1}}{i_{Ls1}} = Z_{p4} \\ G_{p3} = \dfrac{i_{Cg1}}{u_{b1}} = \dfrac{1}{Z_{b1}} \\ G_{p4} = \dfrac{u_{\mathrm{po1}}}{i_{Cg1}} = j\omega_p M_g \\ G_{p5} = \dfrac{i_{Cs1}}{u_{b1}} = \dfrac{1}{Z_{p3}} \end{cases}, \begin{cases} G_{p6} = \dfrac{u_{b2}}{i_{Cs1}} = Z_{p2} \\ G_{p7} = \dfrac{i_{\mathrm{Cg2}}}{u_{b2}} = \dfrac{1}{Z_{b2}} \\ G_{p8} = \dfrac{u_{\mathrm{po2}}}{i_{\mathrm{Cg2}}} = j\omega_p M_g \\ G_{p9} = \dfrac{i_R}{u_{b2}} = \dfrac{1}{j\omega_p L_{s2} + R} \\ G_{p10} = \dfrac{u_R}{i_R} = R \end{cases} \tag{8}$$

where i_{Ls1}, i_{Cg1}, i_{Cs1}, i_{Cg2}, i_R are the currents of L_{s1}, C_{g1}, C_{s1}, C_{g2}, R, respectively. And u_{b1} and u_{b2} are the voltages of the signal branches at the transmitter and receiver sides. $G_{\mathrm{pi}}(\mathrm{i}= 1, \ldots, 10)$ represent the transfer functions of intermediate variables of i_{Ls1}, u_{b1}, i_{Cg1}, i_{Cs1}, u_{b2}, i_{Cg2} and i_R in (8). Based on (7) and (8), the transfer functions from voltage u_{pi} to u_{po1}, u_{po2}, and u_R can be obtained as

$$\begin{cases} G_{\mathrm{transmitter}} = \dfrac{u_{\mathrm{po1}}}{u_{\mathrm{pi}}} = \displaystyle\prod_{i=\{1,2,3,4\}} G_{\mathrm{pi}} \\ G_{\mathrm{receiver}} = \dfrac{u_{\mathrm{po2}}}{u_{\mathrm{pi}}} = \displaystyle\prod_{i=\{1,2,5,6,7,8\}} G_{\mathrm{pi}} \\ G_R = \dfrac{u_R}{u_{\mathrm{pi}}} = \displaystyle\prod_{i=\{1,2,5,6,9,10\}} G_{\mathrm{pi}} \end{cases}. \tag{9}$$

The transfer functions $G_{\mathrm{transmitter}}$ and G_{receiver} represent the power interference on the signal output port on transmitter and receiver sides, respectively. The transfer function G_R presents the gain of power channel without considering the internal components resistances. In the case of the system without signal branches, the transfer function should be equal to one if the internal resistances of the components are ignored. So the difference between G_R considering additional signal branches and G_R without additional signal branches can be adopted to evaluate the interference of the additional signal branches on the power transmission.

IV. Parameters Selection of Signal Channel

For a typical CCPT system with certain parameters and topology on power channel, parameters selection of the signal channel based on the modeling above is a crucial step to ensure the power and signal transmission. Because the transformer is tightly coupled and the coil is winded on the same magnetic core, the coefficient of mutual inductance *k* can be regarded as a constant. Moreover, the variable R_g is seen as a constant, an external resistor R_e is connected to the transformer in series. Then, a constant R_g can be achieved by adopting different R_e. Therefore, only L_g, C_g and λ are concerned as variables to simplify the analysis in (6) and (9).

Based on the analysis in previous sections, in order to achieve the wireless power and signal transfer on a CCPT system, the following three assumptions need to be made:

1) To recognize the signal effectively from power flow, the amplitude of signal voltage u_{so1} and u_{so2} on the output ports have to be much bigger than the amplitude of power interference voltage u_{po1} and u_{po2} on signal output ports.
2) To maintain the power transfer on the CCPT system with signal branches, the gain of power channel G_R from parallel resonant tank voltage to the load voltage have to be larger than a threshold value.
3) In order to ensure that signal 0 and 1 can be distinguished clearly, the gain of the communication channel G_{opposite} have to be larger than a threshold value.

These three assumptions are related to the voltage gain functions in (6) and (9). All the transfer functions are related to the variables L_g, C_g and λ, and the associated constraints can be expressed as

$$\begin{cases} \dfrac{u_{\mathrm{so2}}}{u_{\mathrm{po2}}} = \dfrac{u_{\mathrm{si1}} G_{\mathrm{opposite}}\left(L_g, C_g, \lambda\right)}{u_{\mathrm{pi}} G_{\mathrm{receiver}}\left(L_g, C_g, \lambda\right)} \geq k_e \\ \dfrac{u_{\mathrm{so1}}}{u_{\mathrm{po1}}} = \dfrac{u_{\mathrm{si2}} G_{\mathrm{opposite}}\left(L_g, C_g, \lambda\right)}{u_{\mathrm{pi}} G_{\mathrm{transmitter}}\left(L_g, C_g, \lambda\right)} \geq k_e \\ G_R\left(L_g, C_g\right) \geq G_R^* \\ G_{\mathrm{opposite}}\left(L_g, C_g, \lambda\right) \geq G_{\mathrm{opposite}}^* \end{cases} \tag{10}$$

where k_e is the minimal threshold ratio of the signal voltage u_{so1} and u_{so2} on signal output ports to the power interference voltage u_{po1} and u_{po2} on the signal output ports, respectively. The threshold ratio k_e is adopted to meet the first assumption 1), G_R^* is the minimal gain of power channel which is adopted to meet demand 2), and G_{opposite}^* is the minimal gain of the opposite signal channel which is adopted to meet assumption 3).

V. Ipsilateral Signal Interference Suppression Strategy

In the proposed full-duplex communication system, two signal sources act on the channel simultaneously, so the signal transferred to each side is excited by two separate signal sources on the same channel, they interfere with each other so it is difficult to demodulate the mixed signal directly. To solve the problem, the signal interference between the two signals has to be suppressed. In this section, an ipsilateral signal interference suppression strategy is proposed to eliminate the signal interference.

A. Analysis of Interference and Suppression Principle

Based on the structure shown in Fig. 2, the output signal from port C or port D is stimulated by the two input signals from port A and port B. According to the circuit theory, the signal channel in the proposed topology can be considered as a linear system which satisfies the superposition theorem. It means that the response of the channel with two signal sources equals the algebraic sum of the responses caused by each independent signal source acting alone, where all the other independent

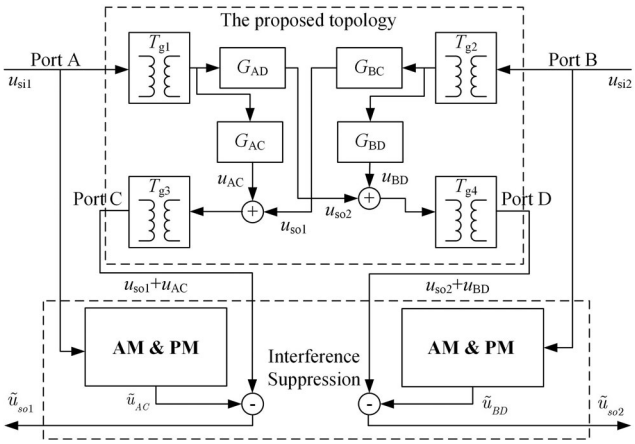

Fig. 5. Block diagram of the interference suppression strategy.

sources are replaced by their internal impedances. However, for the signal pickup, only signal from the input port on opposite side is desired. Contrarily, the signal from ipsilateral side is redundant, moreover, it interferes the opposite signal severely. To obtain the opposite signals effectively, the interference signal from ipsilateral channel have to be suppressed, then the signal from opposite channel can be demodulated. The specific block diagram of proposed method is presented in Fig. 5.

In the block diagram shown in Fig. 5, block G_{AC} and G_{BD} represent the transfer characteristic of ipsilateral signal channel and block G_{AD} and G_{BC} represent the transfer characteristic of opposite signal channel. From port C and D, output signal from both ipsilateral channel and opposite channel can be picked up. To suppress the interference signal from ipsilateral channel, an amplitude modulation and phase modulation Module (AM & PM) are adopted. The specific adjustment value of amplitude and phase are determined by the transfer function $G_{\mathrm{ipsilateral}}$ in (6). Therefore, the estimated output signal from opposite channel can be achieve by

$$\begin{cases} \tilde{u}_{\mathrm{so1}} = (u_{\mathrm{si1}} G_{\mathrm{AC}} + u_{\mathrm{si2}} G_{\mathrm{BC}}) - u_{\mathrm{si1}} G_{\mathrm{ipsilateral}} \\ \tilde{u}_{\mathrm{so2}} = (u_{\mathrm{si1}} G_{\mathrm{AD}} + u_{\mathrm{si2}} G_{\mathrm{BD}}) - u_{\mathrm{si2}} G_{\mathrm{ipsilateral}} \end{cases}. \quad (11)$$

B. AM & PM module

According to the magnitude-frequency and phase-frequency characteristics of the transfer function $G_{\mathrm{ipsilateral}}$ in (6), the relationship of input signal and output signal of ipsilateral channel can be given as

$$u_{\mathrm{so}} = U_{\mathrm{si}} \left| G\left(\omega_s\right) \right| e^{j\varphi(\omega_s)} \quad (12)$$

where $|\mathrm{G}(\boldsymbol{.})|$ and $\varphi(\boldsymbol{.})$ are the magnitude-frequency function and phase-frequency function, respectively. To get the estimated output signal of ipsilateral channel, an *RC* series circuit with amplifier is established as Fig. 6. The signal input u_{si} is set on the *RC* series circuit, and the amplifier increases the voltage amplitude.

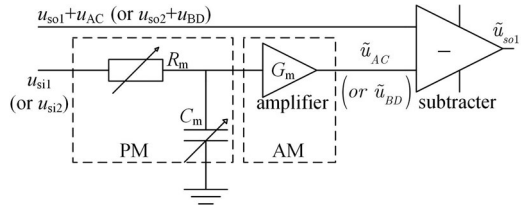

Fig. 6. AM & PM module for the ipsilateral signal channel output estimation.

TABLE I
PARAMETERS OF THE CCPT SYSTEM

Parameters	Values	Parameters	Values
E_{dc}/V	65	L_{dc}/mH	1.00
C_{p}/nF	10.00	L_{p}/μH	10.13
C_{s1}/pF	600.00	C_{s2}/ pF	600
L_{s1}/μH	168.87	L_{s2}/μH	168.87
R/Ω	50	f_{p}/kHz	500

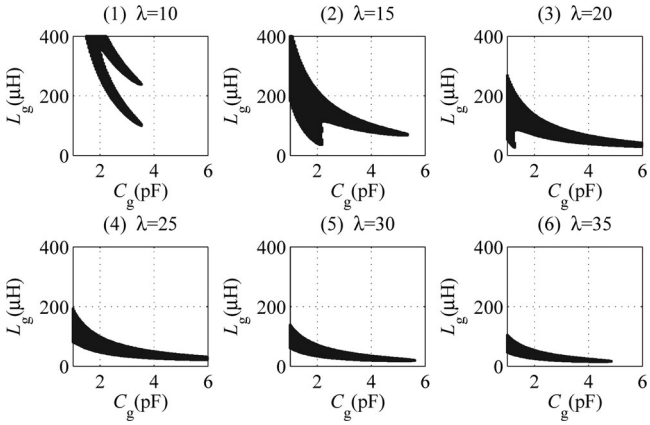

Fig. 7. Feasible region of signal channel parameters selection.

In Fig. 6, the estimated output voltage can be expressed as

$$\tilde{u}_{\mathrm{AC}} = \frac{|G_m|\, U_{\mathrm{si}}}{\sqrt{\left(\omega_s R_m C_m\right)^2 + 1}} e^{[-j\cdot \arctan(\omega_s R_m C_m)]} \quad (13)$$

where $|G_{\mathrm{m}}|$ is the gain of the amplifier. Then, the parameters can be determined as

$$\begin{cases} R_m C_m = -\tan\varphi\left(\omega_s\right)/\omega_s \\ |G_m| = |G\left(\omega_s\right)| \sqrt{\tan^2\varphi\left(\omega_s\right) + 1} \end{cases}. \quad (14)$$

VI. SIMULATION AND EXPERIMENTAL VERIFICATION

In order to verify the proposed topology and interference suppression strategy, MATLAB simulation and practical experimental tests are conducted.

A. Parameters

The parameters of the proposed CCPT system for wireless power transmission (see Fig. 2) under study are shown in Table I.

TABLE II
COMPONENTS PARAMETERS OF THE SIGNAL CHANNEL

Parameters	(1)	(2)	(3)	(4)	(5)	(6)
λ	10	15	20	25	30	35
C_g (pF)	2.5	2.5	5	5	2.5	2.5
L_g (μH)	340	151	42	27	37	28

TABLE III
COMPONENTS PARAMETERS OF PROPOSED TOPOLOGY

Parameters	Values	Parameters	Values
E_{dc}/V	65.0	u_{si1}, u_{si2}/V	10.0
L_g/μH	42.0	C_g/pF	5.0
R_g/Ω	300.0	M_g/μH	37.8

In (10), the coupling coefficient k of the tightly coupled transformer is set at 0.9, the threshold ratio k_e 5, the threshold gain of signal channel is 0.8, the threshold gain of power channel is 0.95, then the values of parameters on a signal branch that satisfy the constraint conditions of (10) can be obtained. The black regions in Fig. 7 show the acceptable values of L_g, C_g and λ.

For different frequency ratios λ, all the combination of parameters L_g and C_g are marked in Fig. 7. Table II presents several suitable parameters with different λ conditions.

Based on the parameters shown in Table II, the Bode magnitude plots of the four transfer functions in (6) and (9) are shown in Fig. 8.

Fig. 8(a) shows the Bode magnitude plots of G_{opposite} function of the opposite signal channel. For each parameters in Table II, the voltage gains on the signal carrier wave frequencies are around the maximal gain point, and they are greater than G^*_{opposite}.

In Fig. 8(b) and (c) show the Bode magnitude plots of $G_{\mathrm{transmitter}}$ and $G_{\mathrm{transmitter}}$ functions of power interference, respectively. The operating frequency points for power transmission are also mark on the curves. On the power resonant frequency, the voltage gain of power interference on signal channel are all smaller than –50 dB.

In Fig. 8(d) shows the Bode magnitude plot of G_{R} function of power transmission from parallel tank to the load. The operating frequency points for power transmission are also marked on the curves. The voltage gain on the resonant frequencies is the maximal gain, and all these voltage gains are close to 0 dB which is the voltage gain for CCPT system without signal branch. It shows that the existence of the signal branch has no observable effect on the WPT.

B. Simulation Results

The proposed topology shown in Fig. 2 has been simulated with MATLAB. The input dc voltage of power is set at 65 V and the component parameters on the main circuit are presented

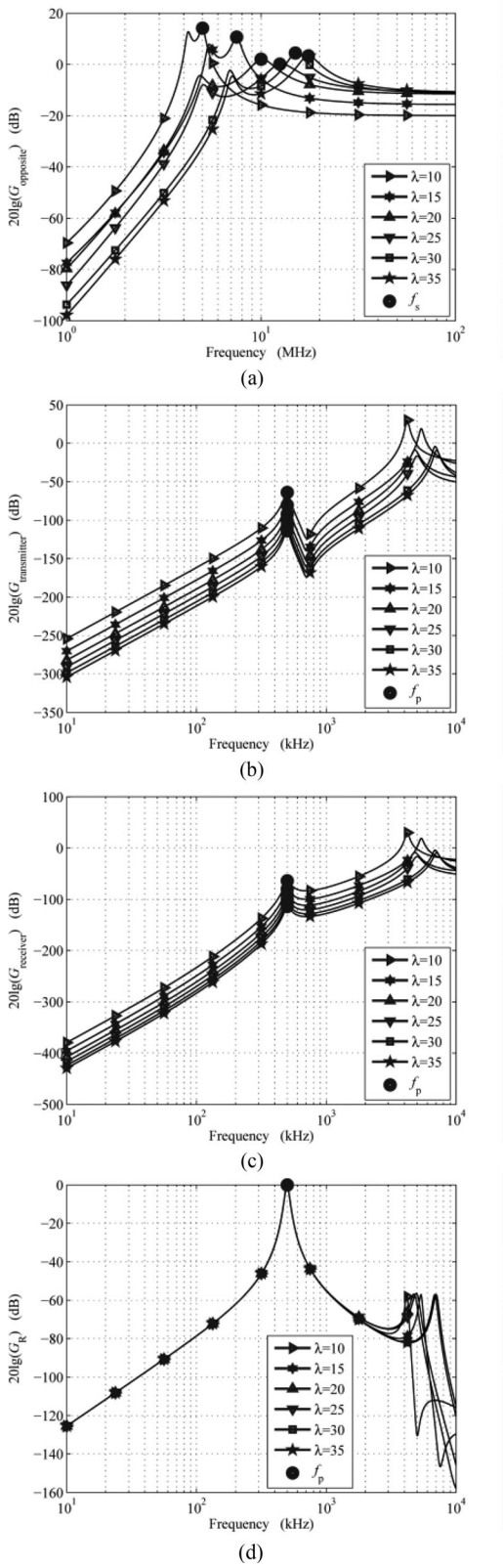

Fig. 8. Frequency response of four transfer functions. (a) The Bode magnitude plot of G_{opposite} function of opposite channel. (b) The Bode magnitude plot of $G_{\mathrm{transmitter}}$ function of power interference. (c) The Bode magnitude plot of G_{receiver} function of power interference. (d) The Bode magnitude plot of G_R function of power transmission.

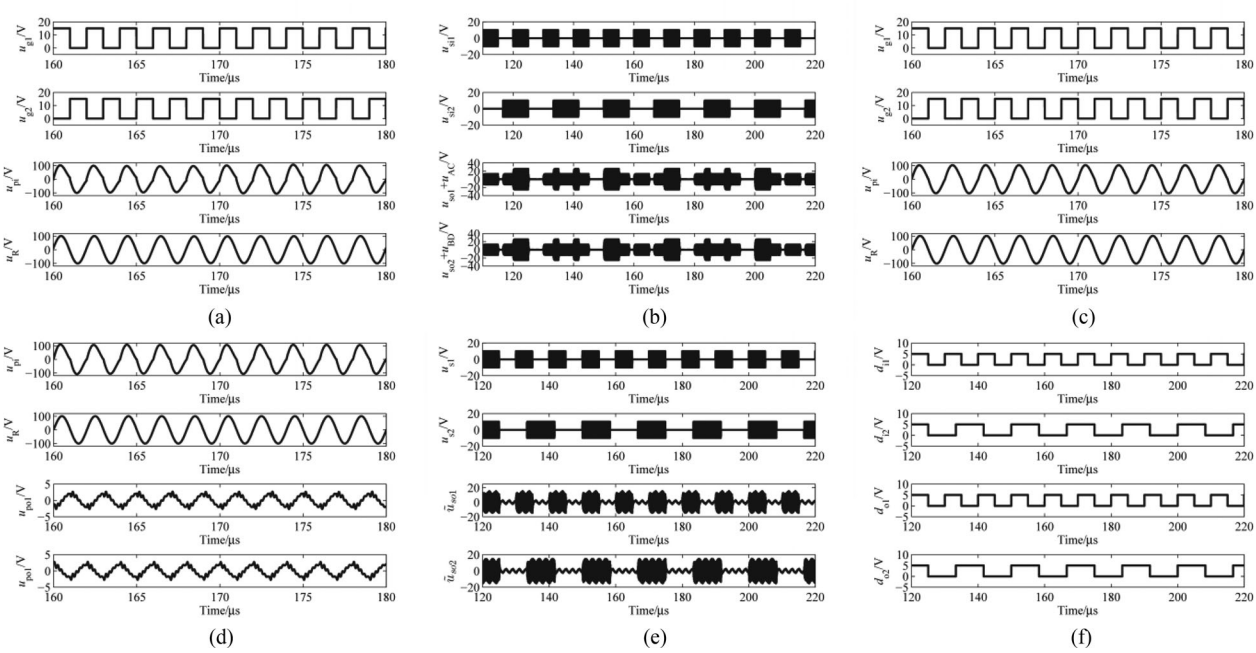

Fig. 9. Simulation waveforms of CCPT system with communication module. (a) The waveforms of traditional CCPT system without signal branch. (b) The waveforms of signal transmission without wireless power transmission. (c) The waveforms of CCPT system with signal branch. (d) The power interference on the signal branch without signal transmission. (e) The waveforms of signal transmission with wireless power transmission synchronously. (f) Modulation and demodulation signals of system.

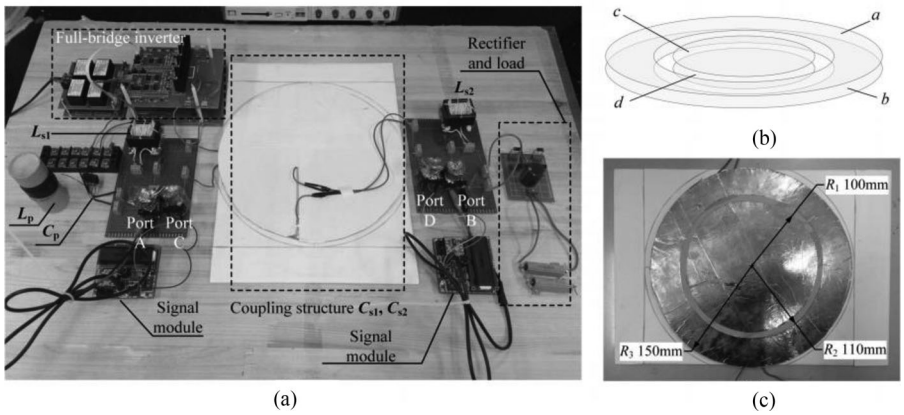

Fig. 10. Experimental setup of the proposed CCPT system. (a) Prototype of the proposed system. (b) Structure chart of the coupling structure (plate *a* and *b* compose the capacitor C_{s1}, plate *c* and *d* compose the capacitor C_{s2}). (c) The actual coupling structure and size.

in Table I, moreover, the selected component parameters on the signal branches are listed in Table II and parameters in the third column of it are chosen for verification. The carrier frequencies of u_{si1} and u_{si2} are both 10.0 MHz. The amplitude of u_{si1} and u_{si2} are both 10 V. The signal modulation frequencies of u_{si1} and u_{si2} are 100 kHz and 60 kHz, respectively.

According to (6), the amplitude attenuation and phase difference can be calculated easily and the results are $|\mathrm{G}| = 1.27, \varphi = 94.84°$, respectively. Substituting the amplitude and phase into (14), the parameters $R_m C_m$ and $|G_m|$ can be derived. Defining the resistor $R_m = 188\ \Omega, C_m = 1\ \mathrm{nF}, |G_m| = 15.1$, then the simulation waveforms of power and signal transmission in the proposed system are presented in Fig. 9.

Fig. 9(a) presents the waveforms of a traditional CCPT system without a signal branch. The first two waveforms are the driving voltages of the MOSFETs $\mathrm{S}_1 - \mathrm{S}_4$ used in the full-bridge inverter. The third waveform is the voltage of parallel resonant tank, the amplitude is 102 V. The fourth waveform is the voltage on the load, the amplitude is 101 V and the output power is 102 W.

Fig. 9(b) shows the waveforms of signal transmission without wireless power transferring. The first waveform is the input signal voltage of transmitter side whose modulation frequency is 100 kHz. The second waveform is the input signal voltage of receiver side whose modulation frequency is 60 kHz. It should be noted that the modulation frequencies of 100 and 60 kHz correspond to baud rates (BRs) of 200 and 120 kb/s, respectively.

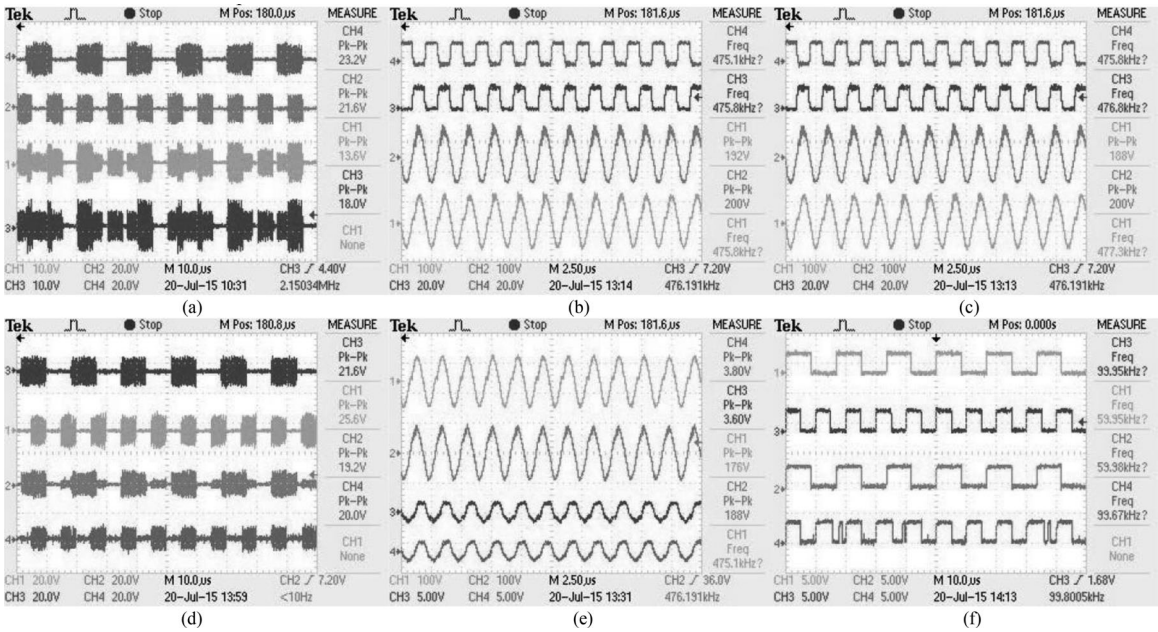

Fig. 11. Experimental waveforms of CCPT system with communication module. (a) The waveforms of traditional CCPT system without signal branch. (b) The waveforms of signal transmission without wireless power transmission. (c) The waveforms of CCPT system with signal branch. (d) The power interference on the signal branch without signal transmission. (e) The waveforms of signal transmission with wireless power transmission synchronously. (f) Modulation and demodulation signals of system.

This is because in a square wave cycle, each high level and low level represents one code cell, so each cycle represents two code cells. The last two waveforms are the output signals of primary and secondary signal branches, respectively.

Fig. 9(c) shows the waveforms of the CCPT system with communication modules. The first two waveforms are the driving voltages of MOSFETs. The third waveform is the voltage of parallel resonant tank and the amplitude is 103 V. The fourth waveform is the voltage on the load, the amplitude is 100 V, and the output power is 100 W which are close to the Fig. 9(a).

In Fig. 9(d) presents the power interference on the signal branch while the wireless power transferring and no signal transferring. The first waveform is the voltage on the parallel resonant tank, the amplitude is 103 V. The second waveform is the voltage on the load, the amplitude is 100 V. The last two waveforms are the voltage on primary and secondary signal branch which are excited by the voltage on the parallel resonant tank. The amplitude of interference voltage of signal output on each side are both 2.4 V.

Fig. 9(e) presents the waveforms of signal transmission with wireless power transferring simultaneously. The first waveform is the input signal voltage of transmitter side whose modulation frequency is 100 kHz. The second waveform is the input signal voltage of receiver side whose modulation frequency is 60 kHz. The third waveform is the output on transmitter side after ipsilateral interference suppression. The fourth waveform is the output on receiver side after ipsilateral interference suppression. The last two waveforms have good correspondence with the first two waveforms which means that the signal can be demodulated after interference suppression.

Fig. 9(f) shows the waveforms of modulation and demodulation signals of the system. The first and the third waveforms $d_{i1},\ d_{i3}$ are the modulate signal of transmitter side and receiver side whose BRs are both 200 kb/s. The second and the fourth waveforms $d_{i2},\ d_{i4}$ are the demodulate signal of transmitter side and receiver side whose bauds rates are both 120 kb/s.

Actually the BR 200 kb/s is a practical maximum value we chose in our simulation analysis and following experimental setup, rather than a theoretical design limit of the system that is mathematically analyzed. At present, the BR of standard serial port communication for industrial applications is between 300 b/s and 115.2 kb/s. In this research, an extra margin of about 85 kb/s above 115.2 kb/s is added to make the maximum 200 kb/s. Our experiments have demonstrated that the proposed communication system can operate at 200 kb/s smoothly.

C. Experimental Results

A practical CCPT experimental setup with the parameters listed in the Tables I and III has been built and tested. The experimental setup of the proposed CCPT system is illustrated in Fig. 10. There are several parts in Fig. 10(a), 1) the full-bridge inverter, 2) the power resonant tank composed by $L_{s1},\ L_{s2},\ L_p$, and C_p, 3) coupling structure C_{s1} and C_{s2}, 4) the rectifier and load, 5) and the signal modules (including the MCU, modulation–demodulation module and AM&PM module). Fig. 10(b) shows the structure chart of coupling structure. This structure can be used in some fixed or rotary devices [28] and its real photo and size are shown in Fig. 10(c). Besides, the distance between the transmitter plates and receiver plates is 1 mm.

TABLE IV
POWER LOSS DISTRIBUTION OF THE SYSTEM

Component	Power loss (%)
Full-bridge inverter	14%
Transmitter side compensating circuit ($C_{\rm p}$, $L_{\rm p}$, and $L_{\rm s1}$)	40%
Coupling plates	18%
Receiver side compensating circuit ($L_{\rm s2}$)	16%
Rectifier and filter capacitor	10%
Communication circuit	2%

TABLE V
PERFORMANCE SUMMARY TABLE OF PROPOSED SYSTEM

Parameters	Values
Power level of CCPT system	100 W
Power efficiency	84%
Signal BR	$<$200 kb/s (covering all the BR of serial port communication)
Bit error rate	0% (when BR$<$200 kb/s)

All the waveforms in the Section VI-B are tested on the practical circuit, and the experimental waveforms are shown in Fig. 11.

By comparing waveforms in Figs. 9 and 11, it can be seen that waveforms of the modulating signal, demodulating signal, carrier wave, and pick-up voltage in the simulation waveforms and experiment waveforms match well to each other, respectively. The simulation waveforms are slightly different from experimental waveforms, as the ultrahigh frequency of the carrier wave increase internal resistance of tightly coupled transformers $T_{g1}-{\rm T}_{\rm g4}$. Therefore, the amplitude of the voltage on detection resistor in Fig. 11(b) is slightly lower than the simulation results in Fig. 9(b). Moreover, the peak resonant voltage [200 V in Fig. 11(a) and 200 V in Fig. 11(c)] and the peak pick-up voltage on the load [192 V in Fig. 11(a) and 188 V in Fig. 11(c)] in Fig. 11(a) and (c) are both slightly lower than the simulation voltage in Fig. 9(a) and (c). The reason is the stray parameters of the elements in the circuit such as internal resistance are not considered in simulation result. In addition, in Fig. 11(f), the demodulation signal waveforms whose BRs are 200 kb/s and 120 kb/s have some unexpected peaks because some abrupt change in the carrier wave affects the demodulation process. However, the unexpected peaks of demodulation signals can be removed by detecting the duration of the high electric level. Therefore, all the differences here have insignificant effect on the system which can be ignored. Besides, the power efficiency is tested and found to be over 84% regardless of whether the branch circuits are added to the original CCPT system. The power loss of the proposed system is analyzed and each part of the loss is listed in Table IV. As can be seen, the whole system is divided into six parts, and the resonant circuits take the highest part of the loss, and the power loss of the communication circuit only takes about 2% of the losses.

The summary performance of the proposed system is listed in Table V.

D. Further Discussion

All the work presented in this paper focuses on the topology and characteristics of the system and the method to transfer power and signal in a shared channel. If a higher data rate is needed in some other applications, the data rate limitation of the proposed system and its influencing factors are also important to measure the capacity of a communication system. Possible limitations of the system include: damping coefficient of the signal channel, effect of the stray parameters, etc. Therefore, the study on the data rate limitation is meaningful for the further research.

VII. CONCLUSION

This paper has proposed a full-duplex communication channel on top of a capacitively coupled WPT system. The working principle of the proposed channel was explained, and the electrical circuit parameters of the channel were calculated based on the analysis of mutual interference between power and signal, as well as the voltage gains on the same channel. In addition, an ipsilateral interference suppression strategy is proposed. After full analysis and design, the system is fully simulated and practically tested. It is demonstrated that 100 W of power can be transferred and a full-duplex communication on the shared channel can be well achieved at 200 kb/s, which is sufficient for normal serial communication applications.

APPENDIX

From Fig. 2, the impedance $Z_{\rm left}$ can be expressed as (A1).

$$Z_{\rm left} = j\omega_s L_{s1} + \frac{j\omega_s L_p}{1-\omega_s^2 L_p C_p}. \tag{A1}$$

According to (1) and (A1), the second term of $Z_{\rm left}$ can be obtained as

$$\frac{j\omega_s L_p}{1-\omega_s^2 L_p C_p} = \frac{j\omega_s L_p}{\omega_p^2 L_p C_p - \omega_s^2 L_p C_p} = \frac{\lambda}{\lambda^2-1}\frac{1}{j\omega_p C_p}. \tag{A2}$$

Because $\lambda \gg 1$, $\lambda/(\lambda^2-1)$ tends to be equal to $1/\lambda$. Because $C_{s1} \ll C_p$ in the practical system, then $L_{s1} \gg L_p$. So that,

$$\begin{aligned} j\omega_s L_{s1} &= j\lambda\omega_p L_{s1} \gg j\lambda\omega_p L_p \gg j\frac{1}{\lambda}\omega_p L_p \\ &= \frac{1}{\lambda}\frac{1}{j\omega_p C_p} \approx \frac{\lambda}{\lambda^2-1}\frac{1}{j\omega_p C_p}. \end{aligned} \tag{A3}$$

Therefore, the second term of $Z_{\rm left}$ can be ignored and $Z_{\rm left}$ can be simplified as

$$Z_{\rm left} = j\omega_s L_{s1}. \tag{A4}$$

Moreover, under the high operating frequency ω_s condition, the impedance of inductor $L_{\rm s2}$ must be much higher than impedance of the equivalent load R in practical system. So that $Z_{\rm right}$ can be obtained as

$$Z_{\rm right} = j\omega_s L_{s2}. \tag{A5}$$

REFERENCE

[1] G. A. Covic and J. T. Boys, "Inductive power transfer," *Proc. IEEE*, vol. 101, no. 11, pp. 1276–1289, Jun. 2013.

[2] J. J. Dai and D. C. Ludois, "A survey of wireless power transfer and a critical comparison of inductive and capacitive coupling for small gap applications," *IEEE Trans. Power Electron.*, vol. 30, no. 11, pp. 6017–6029, Nov. 2015.

[3] H. Hao, G. A. Covic, and J. T. Boys, "A parallel topology for inductive power transfer power supplies," *IEEE Trans. Power Electron.*, vol. 29, no. 3, pp. 1140–1151, Mar. 2014.

[4] Y. G. Su *et al.*, "Steady-state load identification method of inductive power transfer system based on switching capacitors," *IEEE Trans. Power Electron.*, vol. 30, no. 11, pp. 6349–6355, Nov. 2015.

[5] S. Y. R. Hui, W. Zhong, and C. K. Lee, "A critical review of recent progress in mid-range wireless power transfer," *IEEE Trans. Power Electron.*, vol. 29, no. 9, pp. 4500–4511, Sep. 2014.

[6] H. Ishida and H. Furukawa, "Wireless power transmission through concrete using circuits resonating at utility frequency of 60 Hz," *IEEE Trans. Power Electron.*, vol. 30, no. 3, pp. 1220–1229, Mar. 2015.

[7] S. Raju, R. Wu, M. Chan, and C. P. Yue, "Modeling of mutual coupling between planar inductors in wireless power applications," *IEEE Trans. Power Electron.*, vol. 29, no. 1, pp. 481–490, Jan. 2014.

[8] W. M. Ng, C. Zhang, D. Lin, and S. Y. R. Hui, "Two- and three-dimensional omnidirectional wireless power transfer," *IEEE Trans. Power Electron.*, vol. 29, no. 9, pp. 4470–4474, Sep. 2014.

[9] D. C. Ludois, J. K. Reed, and K. Hanson, "Capacitive power transfer for rotor field current in synchronous machines," *IEEE Trans. Power Electron.*, vol. 27, no. 11, pp. 4638–4645, Nov. 2012.

[10] A. P. Hu, C. Liu, and L. L. Hao, "A novel contactless battery charging system for soccer playing robot," in *Proc. 15th Int. Conf. Mechatron. Mach. Vis. Practice*, 2008, pp. 646–650.

[11] K. V. T. Piipponen, R. Sepponen, and P. Eskelinen, "A biosignal instrumentation system using capacitive coupling for power and signal isolation," *IEEE Trans. Biomed. Eng.*, vol. 54, no. 10, pp. 1822–1828, Oct. 2007.

[12] B. H. Choi, D. T. Nguyen, S. J. Yoo, J. H. Kim, and C. T. Rim, "A novel source-side monitored capacitive power transfer system for contactless mobile charger using Class-E converter," in *Proc. IEEE 79th Veh. Technol. Conf.*, 2014, pp. 1–5

[13] F. Lu, H. Zhang, H. Hofmann, and C. Mi, "A double-sided LCLC-compensated capacitive power transfer system for electric vehicle charging," *IEEE Trans. Power Electron.*, vol. 30, no. 11, pp. 6011–6014, Nov. 2015.

[14] W. Y. Lee *et al.*, "Finite-width magnetic mirror models of mono and dual coils for wireless electric vehicles," *IEEE Trans. Power Electron.*, vol. 28, no. 3, pp. 1413–1428, Mar. 2013.

[15] S. Y. Choi, J. Huh, W. Y. Lee, and C. T. Rim, "Asymmetric coil sets for wireless stationary EV chargers with large lateral tolerance by dominant field analysis," *IEEE Trans. Power Electron.*, vol. 29, no. 12, pp. 6406–6420, Dec. 2014.

[16] J. Lee and B. Han, "A bidirectional wireless power transfer EV charger using self-resonant PWM," *IEEE Trans. Power Electron.*, vol. 30, no. 4, pp. 1784–1787, Apr. 2015.

[17] C. Liu, A. P. Hu, and N. K. C. Nair, "Modelling and analysis of a capacitively coupled contactless power transfer system," *IET Power Electron.*, vol. 4, no. 7, pp. 808–815, Aug. 2011.

[18] C. Liu, A. P. Hu, B. Wang, and N. C. Nair, "A capacitively coupled contactless matrix charging platform with soft switched transformer control," *IEEE Trans. Ind. Electron.*, vol. 60, no. 1, pp. 249–260, Jan. 2013.

[19] M. P. Theodoridis, "Effective capacitive power transfer," *IEEE Trans. Power Electron.*, vol. 27, no. 12, pp. 4906–4913, Dec. 2012.

[20] D. C. Ludois, M. J. Erickson, and J. K. Reed, "Aerodynamic fluid bearings for translational and rotating capacitors in noncontact capacitive power transfer systems," *IEEE Trans. Ind. Appl.*, vol. 50, no. 2, pp. 1025–1033, Mar. 2014.

[21] Y. Lim, H. Tang, S. Lim, and J. Park, "An adaptive impedance-matching network based on a novel capacitor matrix for wireless power transfer," *IEEE Trans. Power Electron.*, vol. 29, no. 8, pp. 4403–4413, Aug. 2014.

[22] C. Liu, A. P. Hu, N. C. Nair, and G. A. Covic, "2-D alignment analysis of capacitively coupled contactless power transfer systems," in *Proc. Energy Convers. Congr. Expo.*, 2010, pp. 652–657.

[23] G. X. Wang, P. J. Wang, Y. N. Yi, and W. T. Liu, "Analysis of dual band power and data telemetry for biomedical implants," *IEEE Trans. Biomed. Circuits Syst.*, vol. 6, no. 3, pp. 208–215, Jun. 2012.

[24] Y. L. Li, Y. Sun, and X. Dai, "μ;-synthesis for frequency uncertainty of the ICPT system," *IEEE Trans. Ind. Electron.*, vol. 60, no. 1, pp. 291–300, Jan. 2013.

[25] J. D. Wu, C. W. Zhao, and Z. Y. Lin, "Wireless power and data transfer via a common inductive link using frequency division multiplexing," *IEEE Trans. Ind. Electron.*, vol. 62, no. 12, pp. 7810–7820, Dec. 2015.

[26] Y. Su, W. Zhou, A. P. Hu, C. Tang, and R. Hua, "A shared channel design for the power and signal transfers of electric-field coupled power transfer systems," *J. Power Electron.*, vol. 16, pp. 805–814, Mar. 2016.

[27] C. S. Wang , G. A. Covic, and O. H. Stielau, "Power transfer capability and bifurcation phenomena of loosely coupled inductive power transfer systems," *IEEE Trans. Ind. Electron.*, vol. 51, no. 1, pp. 148–157, Feb. 2004.

[28] C. Liu, A. P. Hu, and N. C. Nair. "Coupling study of a rotary capacitive power transfer system," in *Proc. IEEE Int. Conf. Ind. Technol.*, 2009, pp. 1–6.

Yu-Gang Su (M'09) received the B.E. and M.E. degrees in industry automation and the Ph.D. degree in control theory and control engineering from Chongqing University, Chongqing, China, in 1985, 1993, and 2004, respectively.

From 2008 to 2009, he was a Visiting Scholar in the University of Queensland, Brisbane, Qld., Australia. He is currently a Professor in the College of Automation, Chongqing University. His research interests include power electronics, control theory and applications, and wireless power transfer.

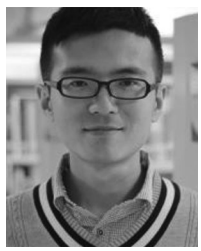

Wei Zhou received the B.E. degree from the College of Automation from Chongqing University, Chongqing, China, in 2013. He is currently working toward the Ph.D. degree in control theory and control engineering from the College of Automation, Chongqing University, China.

His current research interests include capacitively coupled power transfer technology, wireless power and signal parallel transmission, and control theory.

Aiguo Patrick Hu (M'01–SM'07) received the B.E. and M.E. degrees from Xian JiaoTong University, Xi'an, China, in 1985 and 1988, respectively. He received the Ph.D. degree from the University of Auckland, Auckland, New Zealand, in 2001

He served as a Lecturer, the Director of China Italy Cooperative Technical Training Center, Xian, and the General Manager of a technical development company funded by Asian2000 Foundation. He stayed in National University of Singapore for a semester as an Exchange Postdoc Research Fellow. He holds 15 patents in wireless/contactless power transfer and microcomputer control technologies, published more than 200 peer-reviewed journal and conference papers, authored a monograph on wireless inductive power transfer technology, and contributed four book chapters. He is currently with the Department of Electrical and Computer Engineering, University of Auckland, and also the Head of Research of PowerbyProxi Ltd. His research interests include wireless/contactless power transfer systems and application of power electronics in renewable energy systems.

Chun-Sen Tang (S'08–M'09) received the B.E. and Ph.D. degrees in 2004 and 2009 from the College of Automation, Chongqing University, Chongqing, China, respectively.

In 2008, he was a Research Fellow in the Department of Electrical and Computer Engineering, The University of Auckland, Auckland, New Zealand. He joined the College of Automation, Chongqing University, Chongqing, China, in 2009, and is currently an Associate Professor. His current research interests include nonlinear modeling and analysis, intelligent control, and wireless power transfer.

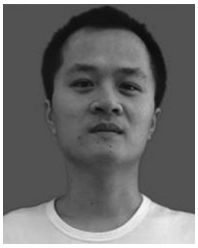

Shi-Yun Xie received the B.E. degree from the College of Automation from Chongqing University, Chongqing, China, in 2010. He is currently working toward the Ph.D. degree in control theory and control engineering from the College of Automation, Chongqing University, Chongqing, China.

His current research interests include mixed-resonant topology of capacitively coupled power transfer systems and its control strategy, and wireless power transfer technologies.

Yue Sun (M'07) received the B.E. degree in electrical engineering, the M.E. degree in industry automation, and the Ph.D. degree in mechanical electrical integrated manufacturing from Chongqing University, Chongqing, China, in 1982, 1988 and 1995, respectively.

In 1997, he was a Senior Visiting Scholar in France for one year. He is currently a Professor in the State Key Laboratory of Power Transmission Equipment & System Security and New Technology, and the College of Automation, Chongqing University, China. His research interests include automatic control, wireless power transfer, and power electronics applications. From 2008 to 2009, he was a Visiting Scholar in the University of Queensland, Brisbane, Qld., Australia. He is currently a Professor in the College of Automation, Chongqing University. His research interests include power electronics, control theory and applications, and wireless power transfer.